

# Separation Efficiency of Particle-Packed HPLC Microchips

Steffen Ehlert,<sup>†</sup> Karsten Kraiczek,<sup>‡</sup> Jose-Angel Mora,<sup>‡</sup> Monika Dittmann,<sup>‡</sup> Gerard P. Rozing,<sup>‡</sup> and Ulrich Tallarek<sup>\*†</sup>

Department of Chemistry, Philipps-Universität Marburg, Hans-Meerwein-Strasse, 35032 Marburg, Germany, and Agilent Technologies GmbH, 76337 Waldbronn, Germany

We report an experimental study of separation efficiency in microchip high-performance liquid chromatography (HPLC). For this study, prototype HPLC microchips were developed that are characterized by minimal dead volume, a separation channel with trapezoidal cross section, and on-chip UV detection. A custom-built stainless steel holder enabled microchip packing under pressures of up to 400 bar and ultrasonication. Bed densities were investigated with respect to the packing conditions and consistently related to pressure drop over the packed microchannels and separation efficiency under isocratic elution conditions. The derived plate height curves show a decrease of mobile phase mass transfer resistance with increasing bed density. High bed densities are critical to separation performance in noncylindrical packed beds, because only at low bed porosities does hydrodynamic dispersion in noncylindrical packings come close to that of cylindrical packings. At higher bed porosities, the presence of fluid channels of advanced flow velocity in the corners of noncylindrical packings affects hydrodynamic dispersion strongly. We demonstrate that the separation channels of HPLC microchips can be packed as densely as the cylindrical fused-silica capillaries used in nano-HPLC and that consequently microchip-HPLC separation efficiencies comparable to those of nano-HPLC can be achieved.

In recent years separation science has witnessed the development of high-performance liquid chromatography (HPLC) at the nanoliter scale. This technological advance was initiated by the ever increasing demand for sensitivity in combination with on-line electrospray ionization mass spectrometric detection (HPLC–ESI/MS).<sup>1–6</sup> Nano-ESI/MS, which refers to ESI performed at flow rates in the range of 200–1000 nL/min, produces smaller droplets than conventional ESI resulting in more efficient ionization. Benefits include greater sensitivity, enhanced dynamic range, and

a reduced competition between analytes for ionization, establishing nano-HPLC–MS as a key technique in proteomics.

A current approach to this technique is microchip-HPLC, where a credit card-sized separation device contains all the functional elements for executing the demanding HPLC separations required in proteomics.<sup>7</sup> Contrary to the cylindrical fused-silica columns used in conventional nano-HPLC, the separation medium on HPLC microchips is contained in a microfluidic channel. Such channels have been fabricated in silicon, glass, quartz, diamond, and a variety of polymeric materials. Their geometry is mainly determined by the fabrication methods used and is usually noncylindrical. Cross sections of microchip separation channels include semicircular, quadratic, rectangular, trapezoidal, and elliptical geometries, often with irregularly angled corners and curved sides. Recent microchips<sup>8–20</sup> use either porous monoliths or slurry-packed particulate beds as separation media. The former have the advantage of easy fabrication by polymerization of the monolithic column directly in the microfluidic channel, whereas the latter are desirable if the wide range of available chromatographic media and the knowledge gained from conventional HPLC is to be utilized. An efficient alternative to the use of packed beds for microchip-HPLC separations may be provided by microfabricated, perfectly ordered pillar array columns.<sup>21–23</sup>

- (7) Coster, S.; Verpoorte, E. *Lab Chip* **2007**, *7*, 1394–1412.
- (8) Xie, J.; Miao, Y.; Shih, J.; Tai, Y.-C.; Lee, T. D. *Anal. Chem.* **2005**, *77*, 6947–6953.
- (9) Lazar, I. M.; Trisripisal, P.; Sarvaiya, H. A. *Anal. Chem.* **2006**, *78*, 5513–5524.
- (10) Yin, H.; Killeen, K.; Brennen, R.; Sobek, D.; Werlich, M.; van de Goor, T. *Anal. Chem.* **2005**, *77*, 527–533.
- (11) Reichmuth, D. S.; Sheppard, T. J.; Kirby, B. J. *Anal. Chem.* **2005**, *77*, 2997–3000.
- (12) Carlier, J.; Arscott, S.; Thomy, V.; Camart, J. C.; Cren-Olivé, C.; Le Gac, S. *J. Chromatogr., A* **2005**, *1071*, 213–222.
- (13) Yang, Y.; Li, C.; Kameoka, J.; Lee, K. H.; Craighead, H. G. *Lab Chip* **2005**, *5*, 869–876.
- (14) Shih, C.-Y.; Chen, Y.; Xie, J.; He, Q.; Tai, Y.-C. *J. Chromatogr., A* **2006**, *127*, 272–278.
- (15) Ro, K. W.; Liu, J.; Knapp, D. R. *J. Chromatogr., A* **2006**, *1111*, 40–47.
- (16) Ishida, A.; Yoshikawa, T.; Natsume, M.; Kamidate, T. *J. Chromatogr., A* **2006**, *1132*, 90–98.
- (17) Bhattacharyya, A.; Klapperich, C. M. *Anal. Chem.* **2006**, *78*, 788–792.
- (18) Mair, D. A.; Geiger, E.; Pisano, A. P.; Fréchet, J. M. J.; Svec, F. *Lab Chip* **2006**, *6*, 1346–1354.
- (19) Wen, J.; Guillo, C.; Ferrance, J. P.; Landers, J. P. *Anal. Chem.* **2007**, *79*, 6135–6142.
- (20) Brio Cartridges, Nanostream, Pasadena, CA.
- (21) De Malsche, W.; Eghbali, H.; Clicq, D.; Vangeloooven, J.; Gardeniers, H.; Desmet, G. *Anal. Chem.* **2007**, *79*, 5915–5926.
- (22) De Pra, M.; De Malsche, W.; Desmet, G.; Schoenmakers, P. J.; Kok, W. J. *Sep. Sci.* **2007**, *30*, 1453–1460.

\* Corresponding author. E-mail: tallarek@staff.uni-marburg.de.

<sup>†</sup> Philipps-Universität Marburg.

<sup>‡</sup> Agilent Technologies.

- (1) Smith, R. D.; Shen, Y. F.; Tang, K. Q. *Acc. Chem. Res.* **2004**, *37*, 269–278.
- (2) Saito, Y.; Jinno, K.; Greibokk, T. *J. Sep. Sci.* **2004**, *27*, 1379–1390.
- (3) Shen, Y. F.; Smith, R. D. *Expert Rev. Proteomics* **2005**, *2*, 431–447.
- (4) Wickremsinhe, E. R.; Singh, G.; Ackermann, B. L.; Gillespie, T. A.; Chaudhary, A. K. *Curr. Drug Metab.* **2006**, *7*, 913–928.
- (5) Manisali, I.; Chen, D. D. Y.; Schneider, B. B. *Trends Anal. Chem.* **2006**, *25*, 243–256.
- (6) Hernández-Borges, J.; Aturki, Z.; Rocco, A.; Fanali, S. *J. Sep. Sci.* **2007**, *30*, 1589–1610.

For a broad acceptance of the microchip-HPLC technology beyond the proteomics community, the separation performance of HPLC microchips should at least equal those of conventional column platforms. A central question that needs to be resolved is how the noncylindrical geometry of the separation channel influences the structure of the packed particulate bed and thus the overall chromatographic performance of the microfluidic chip. Axial dispersion in noncylindrical packings is expected to be affected by the corners of the various conduit geometries which are absent in the classical cylindrical column format. The three-dimensional velocity field and hydrodynamic dispersion in pressure-driven flow through beds of spherical particles have been studied recently by quantitative numerical analysis for conduits with different cross-sectional geometries.<sup>24</sup> This analysis revealed two important aspects which influence hydrodynamic dispersion in noncylindrical compared to cylindrical packings: (i) the presence of corners gives rise to the formation of channels of advanced fluid flow velocity and (ii) the reduced symmetry of noncylindrical packings leads to a longer characteristic length of the solute molecules for lateral equilibration between different velocities. These aspects effect that axial dispersion in noncylindrical packed beds becomes larger than in cylindrical ones of equal cross-sectional area. In addition, noncylindrical packings are affected much stronger by higher bed porosities than cylindrical ones, whereas at low bed porosities hydrodynamic dispersion comes close to that in cylindrical packings.<sup>24</sup>

To corroborate the results from the numerical analysis, the current work presents an experimental investigation of separation efficiencies in microchip-HPLC. For this study, prototype HPLC microchips with minimal dead volume, a separation channel with trapezoidal cross section, and on-chip UV detection were used. Our equipment allowed us to pack the microfluidic channels under pressures of up to 400 bar and ultrasonication. Bed densities (interparticle porosities) of the packed separation channels were investigated with respect to the packing process and correlated to the measured pressure drop and separation efficiencies under isocratic elution conditions. The performance of the microchips is finally compared to that of nanobore-HPLC columns packed with the same adsorbent particles, demonstrating comparable separation efficiencies for both platforms.

## EXPERIMENTAL SECTION

**Chemicals and Materials.** Organic solvents (acetonitrile, methylene chloride, methanol, tetrahydrofuran) and analytes (uracil, benzene, alkylbenzenes) were purchased from Sigma-Aldrich Chemie GmbH (Taufkirchen, Germany). HPLC grade water was prepared using a Milli-Q gradient water purification system (Millipore, Bedford, MA). The packing material was 5  $\mu\text{m}$  sized Zorbax SB-C18 with a mean intraparticle pore size of 80  $\text{\AA}$  (Agilent Technologies, Waldbronn, Germany). Measurement of the size distribution provided a Sauter mean diameter of  $5.51 \pm 0.12 \mu\text{m}$  for these particles,<sup>25</sup> which were slurry-packed into prototype HPLC/UV microchips.

**Microchip Design and On-Chip UV Detection.** The prototype HPLC/UV microchips consist of a three-layered, laminated

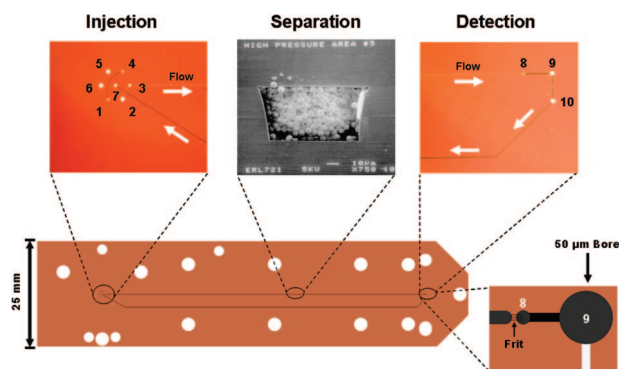


**Figure 1.** Layout of the polyimide-based microchips employed for the study of packing density and separation efficiency in microchip-HPLC. The design integrates sample injection, HPLC separation in a packed bed with trapezoidal cross section, and UV detection.

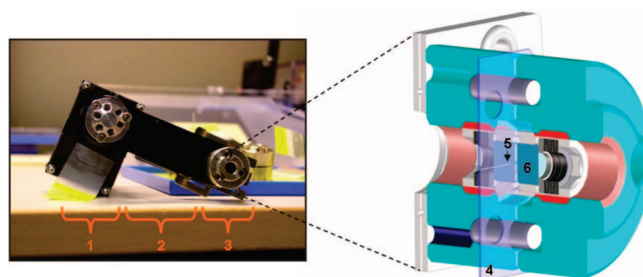


**Figure 2.** Final assembly of an HPLC microchip between rotary valve and UV detection cell. The numbers indicate the following: 1, injection; 2, separation; 3, detection; 4, fixed microchip; 5, particle-packed separation channel; 6, sapphire window (3 mm thick).

polyimide design and integrate the following three operational elements: injection, separation, and detection (Figure 1). Additional fabrication details of these flexible polymer microchips can be found in a recent publication.<sup>10</sup> Due to the use of laser-cut polyimide foils the cross-sectional shape of the separation channels in the resulting three-layered, laminated design is trapezoidal. For sample injection the microchips were connected to a face-seal rotary valve with a 0.7 nL internal loop between ports 1 and 4 (Figure 1). Each port contributed another 2.2 nL to the sample load. Sample is injected without dead volume onto the packed bed in the separation channel. This separation channel between ports 3 and 8 has a  $75 \mu\text{m} \times 50 \mu\text{m}$  trapezoidal cross section and typically a length of 75 mm. A micromachined outlet frit was used to retain the packing at the end of the separation channel. On-chip UV detection occurred behind the outlet frit with a prototype UV cell of 50  $\mu\text{m}$  i.d. and 300  $\mu\text{m}$  path length (port 9) which was connected to the diode array detector with a special holder (Figure 2). The dead volume between outlet frit and detection cell (ports 8 and 9) was 2.5 nL. Thus, the overall dead volume passed by the analytes from injection to detection is negligible compared to the volume of the empty separation channel of about 260 nL. Behind the detector the mobile phase is redirected via ports 10 and 7 to an external flow sensor.

**Microchip Packing.** Slurries of 50 mg of the dry particles were prepared in ca. 1 mL of tetrahydrofuran. Methanol was used as pushing solvent in the packing process.<sup>26</sup> Microchips were tightly fixed in a custom-built stainless steel holder and connected

(23) Billen, J.; Desmet, G. J. *Chromatogr., A* **2007**, *1168*, 73–99.

(24) Khirevich, S.; Hölzel, A.; Hlushkou, D.; Tallarek, U. *Anal. Chem.* **2007**, *79*, 9340–9349.

(25) Ehler, S.; Rösler, T.; Tallarek, U. *J. Sep. Sci.* **2008**, *31*, 1719–1728.

to the packing station via port 3 (Figure 1). For the application of high pressure a WellChrom K-1900 pneumatic pump (Knauer GmbH, Berlin, Germany) with a 500  $\mu\text{m}$  i.d. glass-lined metal tubing as slurry reservoir was used. After filling the slurry reservoir microchips were inserted into an ultrasonic bath. By applying ultrasound and pressures of up to 400 bar the packing procedure was started and maintained for 7 min. Then, ultrasound was switched off and the system slowly depressurized which took at least 15 min. Alternatively, the separation channels were packed under high pressure only, without ultrasound assistance. Afterward, the microchips were disconnected, inspected microscopically for gaps in the packing and damages in general, and then attached to the injection valve and special UV holder (see final assembly in Figure 2) for the subsequent studies of interparticle porosity and separation efficiency.

**Packing Densities and Separation Efficiencies.** Packing densities in the separation channels of the microchips were analyzed with the help of inverse size exclusion chromatography.<sup>25</sup> The interparticle pore volume ( $V_{\text{inter}}$ ) of the packed microchips was calculated using the elution volumes in methylene chloride of a small polystyrene standard ( $M_r = 20\,000$ ) that is just size-excluded from the intraparticle pore space of the employed C18-silica particles. The interparticle porosity ( $\varepsilon_{\text{inter}}$ ) was then calculated by  $\varepsilon_{\text{inter}} = V_{\text{inter}}/V_{\text{ch}}$  where  $V_{\text{ch}}$  is the volume of the empty separation channel measured prior to the microchip packing. Separation efficiencies were analyzed by isocratic elution of a mixture of alkylbenzenes with acetonitrile/water 80/20 (v/v) and uracil as dead-time marker. This complementary analysis allowed us to correlate the packing procedure for the microchips with the achieved packing densities and separation efficiencies. Plate heights were calculated with the ChemStation software and were found, not least due to the generally high symmetry of the peaks, practically identical to those obtained by the method of moments (via the second central moment). The error in the determination of  $\varepsilon_{\text{inter}}$  was on the order of 1%.

**Hardware Configuration.** All data were acquired with an Agilent 1200 liquid chromatograph, including a degasser and a nanopump, equipped with a diode array UV detector. Microchips were sandwiched between the stator and the rotor of a two-position HPLC rotary valve (Figure 2). Volumetric flow rates were controlled by an additional flow sensor (model SLG-1430-150 from Sensirion, Staefa, Switzerland) installed behind the analytical system (behind port 7, see Figure 1). Packing densities (interparticle porosities) were analyzed with methylene chloride as mobile phase and detection at 230 nm, whereas separation efficiencies were analyzed with acetonitrile/water 80/20 (v/v) as mobile phase and detection at 210 nm. All experiments were carried out at  $298 \pm 1$  K.

## RESULTS AND DISCUSSION

Microchips of the design illustrated in Figures 1 and 2 and packed under different conditions were studied by chromatographic separations of a mixture of alkylbenzenes (Figure 3a) at different mobile phase velocities. The peak shapes observed in the chromatograms were generally very symmetrical, with typical asymmetry factors around 1.1. Separation efficiencies of the

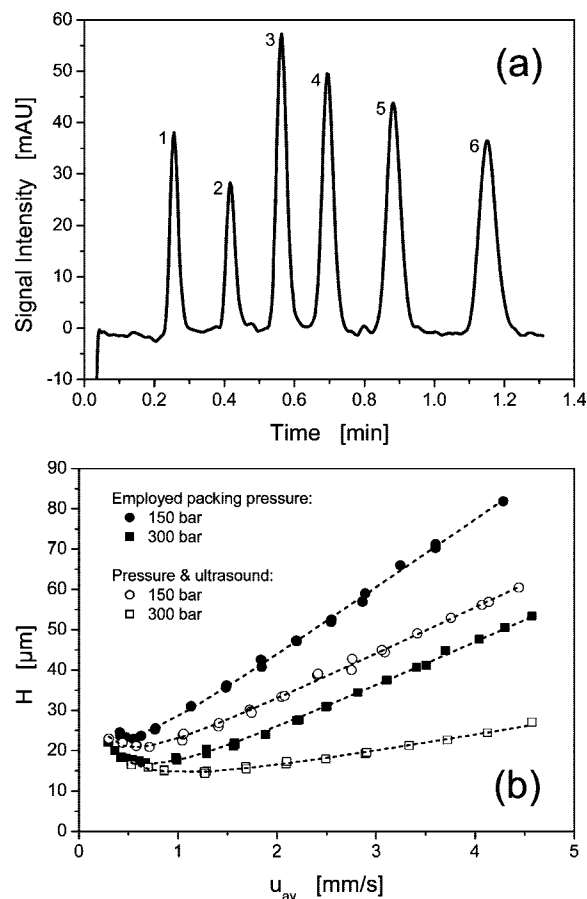


**Figure 3.** (a) Separation of alkylbenzenes ( $u_{\text{av}} = 4.6$  mm/s) using the microchip packed at 300 bar and with the assistance of ultrasound (see panel b, bottom curve, last point for pentylbenzene). Analytes (asymmetry factors) are the following: 1, uracil (0.97); 2, benzene (1.20); 3, ethylbenzene (1.06); 4, propylbenzene (1.25); 5, butylbenzene (1.04); 6, pentylbenzene (1.14). (b) Plate height vs average mobile phase velocity for microchips packed at different pressures, with or without the assistance of ultrasound. Mobile phase, acetonitrile/water 80/20 (v/v); analyte, pentylbenzene ( $k' = 3.5$ ).

microchips were analyzed by the axial plate height calculated from the pentylbenzene peak ( $k' = 3.5$ ) in the chromatograms. Figure 3b shows the dependence of axial plate height ( $H$ ) on the average mobile phase velocity ( $u_{\text{av}}$ ) for microchips packed under different conditions. It is evident that both packing pressure (150  $\rightarrow$  300 bar) and the application of ultrasound are critical to obtaining good separation efficiencies. The chromatogram shown in Figure 3a was acquired at the highest mobile phase velocity ( $u_{\text{av}} = 4.6$  mm/s) with the best-performing microchip packed at 300 bar and with ultrasound assistance, resulting in an axial plate height of  $H = 25$   $\mu\text{m}$  for pentylbenzene (cf. Figure 3b).

The improvement in separation efficiency demonstrated in Figure 3b of microchips packed at higher pressure (150  $\rightarrow$  300 bar) and with ultrasound assistance is significant, by a factor of more than 3 for velocities above  $u_{\text{av}} = 4$  mm/s. Packing pressures of up to 400 bar were investigated, with and without ultrasound assistance, but did not result in a further improvement of separation efficiencies. Although Figure 3b reveals also a decrease in the minimum plate height from 23  $\mu\text{m}$  at  $u_{\text{av}} = 0.55$  mm/s for the microchip packed at 150 bar to 14  $\mu\text{m}$  at  $u_{\text{av}} = 1.25$  mm/s for the one packed at 300 bar and with ultrasound assistance, the

(26) Vissers, J. P. C.; Claessens, H. A.; Laven, J.; Cramers, C. A. *Anal. Chem.* **1995**, *67*, 2103–2109.

strongest effect is seen at increasing velocities (for  $u_{av} > 1$  mm/s) in a strongly reduced slope of the plate height curve. With the best-performing microchip (300 bar/ultrasound) we observe a relatively broad minimum and weak increase in plate heights for  $u_{av} > 1.5$  mm/s. This behavior indicates that the contribution to the plate height from mass transfer resistance in the mobile phase (which scales linearly with the average velocity) is very sensitive to the packing procedure used for the microchips.

A possible reason for this behavior can be found in the channeling of fluid flow in the corners of noncylindrical, here trapezoidal, packings, which is expected to depend critically on the packing density. It has been demonstrated that the morphologies and corresponding flow patterns for noncylindrical packings can deviate significantly from those of conventional cylindrical packings.<sup>24</sup> This deviation becomes more pronounced at higher bed porosities (lower packing densities). Extended regions of high local porosity in the corners of noncylindrical conduits give rise to the formation of fluid channels of advanced flow velocity, whereas at lower bed porosities (higher packing densities) hydrodynamic dispersion comes close to that of the cylindrical packings.<sup>24</sup>

In order to verify this hypothesis we analyzed the packing densities of the microchips by their interparticle porosity ( $\epsilon_{inter}$ ), using a suitable polystyrene standard in methylene chloride which is size-excluded from the intraparticle pore space of the packing.<sup>25</sup> We found a consistent decrease in  $\epsilon_{inter}$  of the microchips with increasing separation efficiency, that is,  $\epsilon_{inter}$  decreased in the following series of packing modes: 150 bar > 150 bar/ultrasound > 300 bar > 300 bar/ultrasound. The more densely a microchip is packed, the better it performs. In Figure 4a plate height data at selected mobile phase velocities from Figure 3b are correlated to the actual values of  $\epsilon_{inter}$ . For example, at a velocity of  $u_{av} = 3.7$  mm/s (open circles) we observe a decrease in plate height by a factor of about 3 from the microchip packed at 150 bar ( $\epsilon_{inter} = 0.475$ ) to the one packed at 300 bar and with ultrasound assistance ( $\epsilon_{inter} = 0.423$ ). These complementary data confirm that the improvement in separation efficiency (Figure 3b) can be explained by higher packing densities (Figure 4a) achieved by the increased packing pressure and simultaneous application of ultrasound.

As mentioned above, the corners of a noncylindrical cross section favor the formation of channels of advanced fluid flow velocity. A denser packing reduces the extension of these channels as well as the actual fluid velocity in these channels.<sup>24</sup> Thus, associated hydrodynamic dispersion can be reduced significantly by a denser packing. The numerical analysis of a conduit with semicircular cross section, which has a symmetry comparable to the trapezoidal one encountered in this work, revealed a reduction of the axial dispersion coefficient by a factor of about 3 at a reduced velocity of  $u_{av}d_p/D_m = 20$  (where  $d_p$  is the particle diameter and  $D_m$  the tracer diffusivity in the mobile phase) when the interparticle porosity was decreased from  $\epsilon_{inter} = 0.48$  to  $\epsilon_{inter} = 0.42$ .<sup>24</sup> At least from a macroscopic hydrodynamic viewpoint these predictions, which are based on the numerical simulation of flow and dispersion in noncylindrical sphere packings, reflect closely the experimental data presented in this work for a similar velocity. The reduced velocity of  $u_{av}d_p/D_m = 20$  in the simulations translates to an  $u_{av}$  of ca. 4 mm/s in this work. Around this velocity

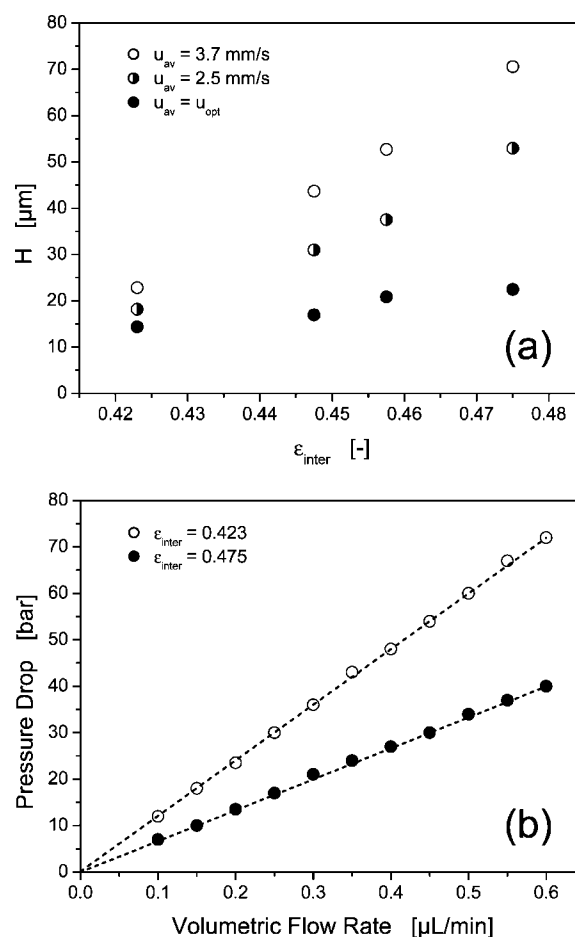


**Figure 4.** (a) Dependence of plate height at selected mobile phase velocities on the interparticle porosity of packed microchips.  $u_{opt}$  refers to the minimum in the plate height curves of Figure 3b. Mobile phase, acetonitrile/water 80/20 (v/v); analyte, pentylbenzene ( $K = 3.5$ ). (b) Pressure drop over the length of the packed separation channel (75 mm) vs volumetric flow rate. The lower packing density ( $\epsilon_{inter} = 0.475$ ) characterizes the microchip packed at 150 bar;  $\epsilon_{inter} = 0.423$  corresponds to the one packed at 300 bar and with ultrasound assistance (cf. Figure 3b).

the data in Figures 3b and 4a show a reduction of the plate height (dispersion coefficient) by a factor of about 3 as the interparticle porosity is decreased from  $\epsilon_{inter} = 0.475$  (microchip packing at 150 bar) to  $\epsilon_{inter} = 0.423$  (300 bar and ultrasound), comparable to the simulated data.

In addition, a porosity-dependent intensity of the channeling in the corners of the trapezoidal packed beds well explains the different slopes of the plate height curves in Figure 3b (150 bar vs 300 bar and ultrasound). The corner regions act as more permeable flow paths parallel to the more densely packed bed (parallel combination of unequal resistances) over the entire length of the bed. Lateral equilibration is diffusion-limited, and therefore, this macroscopic flow heterogeneity engenders mass transfer resistance in the mobile phase over relatively long distances (requiring transcolumen equilibration).<sup>24,27</sup>

The higher packing density in microchips not only effects better separation efficiencies but also leads to an expected increase in pressure drop at a given flow rate, as illustrated in Figure 4b. Although we observe a linear pressure drop–flow rate charac-

(27) Broeckhoven, K.; Desmet, G. J. *Chromatogr., A* **2007**, *1172*, 25–39.

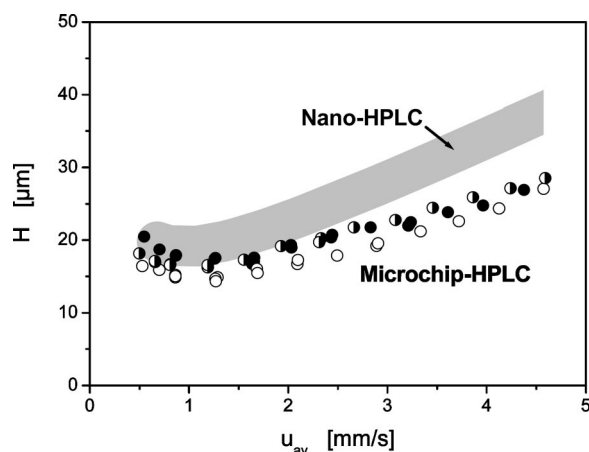


**Figure 5.** Comparison of plate height curves in nano-HPLC and microchip-HPLC employing 50 and 75  $\mu\text{m}$  i.d. cylindrical fused-silica capillaries and polyimide-based microchips with a ca. 50  $\mu\text{m} \times 75 \mu\text{m}$  trapezoidal cross section, respectively, packed with the same particles (5  $\mu\text{m}$  sized Zorbax SB-C18). The three microchip packings (circles) have been prepared with 300 bar as packing pressure and ultrasound assistance. Mobile phase, acetonitrile/water 80/20 (v/v); analyte, pentylbenzene ( $K' = 3.5$ ).

teristic for both densely and more loosely packed microchips ( $\epsilon_{\text{inter}} = 0.423$  and  $\epsilon_{\text{inter}} = 0.475$ ), reflecting the validity of Darcy's law, the actual increase in pressure drop for the denser packed microchip can be well explained on the basis of the Kozeny–Carman equation,<sup>28</sup> which correlates pressure drop to the porosity function  $(1 - \epsilon_{\text{inter}})^2 / \epsilon_{\text{inter}}^3$ .

The interparticle porosity of microchips packed at 300 bar and with ultrasound assistance ( $\epsilon_{\text{inter}} \approx 0.42$ ) characterizes packing densities very close to those realized in nano-HPLC columns packed with the same particles.<sup>25</sup> In particular, we found  $\epsilon_{\text{inter}} = 0.41$ – $0.43$  for 50 and 75  $\mu\text{m}$  i.d. cylindrical fused-silica capillary columns packed with the Zorbax particles used in this study. These capillaries were packed following optimized protocols available in the literature. It means that with the current equipment the microchips can be packed as densely as conventional columns in nano-HPLC with a comparable column-to-particle size ratio. This is an important finding because microchip packing is not a firmly established procedure but still retains an experimental character: microchannels are often filled manually with a syringe or the help of pumps at low to moderate pressure. We show that, in principle, noncylindrical packings in microchip-HPLC can be prepared as densely as the cylindrical ones routinely used in nano-HPLC.

An important conclusion from this fact is that the separation efficiencies of the noncylindrical packed beds in microchip-HPLC should become similar to those achieved with the cylindrical packings in nano-HPLC.<sup>24</sup> Figure 5 compares plate height data generated with the packed microchips to those realized with 50 and 75  $\mu\text{m}$  i.d. cylindrical fused-silica capillaries packed with the same particles.<sup>25</sup> The complete range spanned by the plate height data for these nano-HPLC columns is represented by the gray-shaded area. The microchips used in this comparison (circles) have been packed at 300 bar and with ultrasound assistance reflecting the best packing conditions realized in this work (cf.

Figure 3b). All packed-bed structures gave interparticle porosities of  $\epsilon_{\text{inter}} = 0.41$ – $0.43$  and are, thus, comparable in this regard. In addition, the packed microchips, which were taken from different fabrication batches, demonstrate a good reproducibility concerning separation efficiencies in combination with the packing process. It should be stressed that in this comparison of separation efficiency in nano-HPLC and microchip-HPLC similar separation channel-to-particle size ratios have been employed, the same particles have been used for preparing all packed beds, and comparable packing densities have been considered. This avoids biases which generally may be introduced by the influence of particle characteristics<sup>29,30</sup> (e.g., their size and shape distribution functions or surface roughness), the separation channel-to-particle size ratio<sup>25,31,32</sup> (due to the operation of a geometrical wall effect), and the packing density<sup>24</sup> on hydrodynamic dispersion.

Although the plate height data in nano-HPLC and microchip-HPLC are generally close, especially around the plate height minimum ( $u_{\text{av}} = 1.0$ – $1.5$  mm/s), the microchips even demonstrate a slightly better performance at increasing mobile phase velocities ( $u_{\text{av}} > 2$  mm/s). We attribute this finding to the preparation (sintering) of inlet and outlet frits in the case of the packed capillaries. Packed capillaries were cut at the inlet frit and connected directly to the injection valve, and the detection window was prepared immediately behind the outlet frit.<sup>25</sup> Thus, the dead volume for the nano-HPLC configuration was minimized, as in the microchip-HPLC studies (cf. the Experimental Section). Sintered frits are known as a possible source of structural inhomogeneities which increase band broadening.<sup>33–35</sup> The retaining filter and frit elements of microchips can be micromachined more precisely, homogeneously, and reproducibly than frits can be sintered over the whole cross section of the capillaries, which may explain the slightly better performance of microchip-HPLC compared to nano-HPLC demonstrated by Figure 5.

## CONCLUSIONS

This work provides an experimental analysis and consistent interrelation of the packing procedure, resulting packing density (interparticle porosity), pressure drop over the packed microchannel, and separation efficiency under isocratic elution conditions for noncylindrical packed beds employed in microchip-HPLC. In particular, the present work demonstrates that the separation channels of suitable microfluidic analysis systems, which often cannot tolerate the high packing pressures used in conventional column packing and the application of ultrasound, can be packed as densely as the cylindrical fused-silica capillaries commonly used in nano-HPLC. This progress was realized with a stainless steel envelope which tightly fixed the flexible polymeric microchips during the packing process, allowing the application of packing pressures of up to 400 bar with ultrasound assistance. The achieved packing densities were comparable to those in nano-HPLC for capillary columns characterized by similar column-to-

(29) Billen, J.; Guillaume, D.; Rudaz, S.; Veuthey, J.-L.; Ritchie, H.; Grady, B.; Desmet, G. *J. Chromatogr., A* **2007**, *1161*, 224–233.

(30) Gritti, F.; Guiochon, G. *J. Chromatogr., A* **2007**, *1166*, 30–46.

(31) Kennedy, R. T.; Jorgenson, J. W. *Anal. Chem.* **1989**, *61*, 1128–1135.

(32) Hsieh, S.; Jorgenson, J. W. *Anal. Chem.* **1996**, *68*, 1212–1217.

(33) Tang, Q.; Lee, M. L. *Trends Anal. Chem.* **2000**, *19*, 648–663.

(34) Piraino, S. M.; Dorsey, J. G. *Anal. Chem.* **2003**, *75*, 4292–4296.

(35) Zhang, B.; Bergström, E. T.; Goodall, D. M.; Myers, P. *Anal. Chem.* **2007**, *79*, 9229–9233.

(28) Bear, J. *Dynamics of Fluids in Porous Media*; Dover Publications: New York, 1988.

particle size ratios as the trapezoidal microchip separation channels when packed with the same particles.

To realize the dense packing in microchip separation channels that is crucial to achieve good separation efficiency, it is necessary to optimize packing procedures, and in this respect the development of high-pressure-rating microchannels and fittings is particularly desirable. As a consequence of the denser packing the separation efficiencies in microchip-HPLC with noncylindrical packed beds approach those realized with the cylindrical packed beds used in conventional nano-HPLC. This behavior was predicted by numerical simulations<sup>24</sup> and is explained by the presence of fluid channels of advanced flow velocity in the corners of noncylindrical packed beds. Noncylindrical packings are therefore affected much stronger by higher bed porosities than cylindrical ones, whereas at low bed porosities hydrodynamic dispersion

comes close to that of the cylindrical packings as demonstrated experimentally in this work. With optimized particle packing in the separation channels the microchip-HPLC platform benefits from a seamless integration of functional elements and the precision possible with micromachining technology.

#### **ACKNOWLEDGMENT**

The work of Steffen Ehlert was supported by an Agilent Technologies Ph.D. Fellowship award through the University Relations Ph.D. Fellowship program. We thank Dr. Alexandra Höltzel for her help in preparing this manuscript.

Received for review March 20, 2008. Accepted April 30, 2008.

AC800576V